ISSN 1674-1056
http://cpb.iphy.ac.cn
http://iopscience.iop.org/cpb
中国物理 B
Chinese Physics
中国物理 Chinese Physics B

Influence factors of electromagnetic scattering from dielectric periodic surface

Yinyu Wei(韦尹煜), Zhensen Wu(吴振森), Haiying Li(李海英), Jiaji Wu(吴家骥), Tan Qu(屈檀)

Citation: Chin. Phys. B . 2019, 28(7): 074101. **doi:** 10.1088/1674-1056/28/7/074101
Journal homepage: http://cpb.iphy.ac.cn; http://iopscience.iop.org/cpb

What follows is a list of articles you may be interested in

Nonreciprocal transmission of electromagnetic waves by three-layer magneto-optical mediums

Guan-Xia Yu(余观夏), Jing-Jing Fu(付晶晶), Wen-Wen Du(杜文文), Yi-Hang Lv(吕一航), Min Luo(骆敏)
Chin. Phys. B . 2019, 28(2): 024101. **doi:** 10.1088/1674-1056/28/2/024101

Homogeneous transparent device and its layered realization

Cheng-Fu Yang(杨成福), Ming Huang(黄铭), Jing-Jing Yang(杨晶晶), Fu-Chun Mao(毛福春), Ting-Hua Li(李廷华), Peng Li(黎鹏), Peng-Shan Ren(任鹏姗)
Chin. Phys. B . 2018, 27(12): 124101. **doi:** 10.1088/1674-1056/27/12/124101

Polarization ratio characteristics of electromagnetic scattering from sea ice in polar areas

Li Zhao(赵立), Tao Xie(谢涛), Lei Meng(孟雷), William Perrie, Jin-Song Yang(杨劲松), He Fang(方贺), Han Chen(陈韩), Run-Bing Ai(艾润冰)
Chin. Phys. B . 2018, 27(12): 124102. **doi:** 10.1088/1674-1056/27/12/124102

Ultra-wideband low radar cross-section metasurface and its application on waveguide slot antenna array

Li-Li Cong(丛丽丽), Xiang-Yu Cao(曹祥玉), Tao Song(宋涛), Jun Gao(高军)
Chin. Phys. B . 2018, 27(11): 114101. **doi:** 10.1088/1674-1056/27/11/114101

Design of multi-band metasurface antenna array with low RCS performance

Si-Ming Wang(王思铭), Jun Gao(高军), Xiang-Yu Cao(曹祥玉), Yue-Jun Zheng(郑月军), Tong Li(李桐), Jun-Xiang Lan(兰俊祥), Liao-Ri Ji-Di(吉地辽日)
Chin. Phys. B . 2018, 27(10): 104102. **doi:** 10.1088/1674-1056/27/10/104102

Factors influencing electromagnetic scattering from the dielectric periodic surface*

Yinyu Wei(韦尹煜)[1], Zhensen Wu(吴振森)[1,2,†], Haiying Li(李海英)[1], Jiaji Wu(吴家骥)[3], and Tan Qu(屈檀)[3]

[1] School of Physics and Optoelectronic Engineering, Xidian University, Xi'an 710071, China
[2] Collaborative Innovation Center of Information Sensing and Understanding, Xidian University, Xi'an 710071, China
[3] School of Electronic Engineering, Xidian University, Xi'an 710071, China

(Received 8 January 2019; revised manuscript received 2 April 2019; published online 21 May 2019)

The scattering characteristics of the periodic surface of infinite and finite media are investigated in detail. The Fourier expression of the scattering field of the periodic surface is obtained in terms of Huygens's principle and Floquet's theorem. Using the extended boundary condition method (EBCM) and T-matrix method, the scattering amplitude factor is solved, and the correctness of the algorithm is verified by use of the law of conservation of energy. The scattering cross section of the periodic surface in the infinitely long region is derived by improving the scattering cross section of the finite period surface. Furthermore, the effects of the incident wave parameters and the geometric structure parameters on the scattering of the periodic surface are analyzed and discussed. By reasonable approximation, the scattering calculation methods of infinite and finite long surfaces are unified. Besides, numerical results show that the dielectric constant of the periodic dielectric surface has a significant effect on the scattering rate and transmittance. The period and amplitude of the surface determine the number of scattering intensity peaks, and, together with the incident angle, influence the scattering intensity distribution.

Keywords: periodic surface, Floquet's theorem, extended boundary condition method (EBCM), scattering cross section, energy conservation

PACS: 41.20.Jb, 41.20.–q **DOI:** 10.1088/1674-1056/28/7/074101

1. Introduction

The initial theoretical research of the periodic surface scattering was delivered by Lord Rayleigh,[1,2] and the Rayleigh approach has attracted continuous attention due to its high efficiency. Based on this theory, the reflection of scalar plane waves from the periodic surface is studied. Uretsky[3] paid attention to the sinusoidal conductor surface upon which the wave function vanished, and found that the matrix of reflection coefficients for an arbitrary periodic nonabsorbing surface has interesting symmetry properties, which are reminiscent of the quantum mechanical S-matrix. In 1974, Desanto[4] constructed the scattering field for a plane wave incident on a sinusoidal surface, and extended exact analysis of plane wave scattering from a sinusoidal surface to the case of an arbitrary periodic surface.[5] In 1979, Jordan[6] presented the scattering patterns from sinusoidal surfaces. An asymptotic evaluation was employed to obtain an exact expression for the scattering pattern as a product of the space harmonic scattering coefficients times the corresponding pattern functions. In 1980, Wang[7] utilized the theory of scattering and propagation of the periodic surface to study the effect of row structure on the microwave emission from a bare agricultural field.

Chuang and Kong proposed a method on the basis of Waterman's extended boundary condition approach, and applied this theory to the study of laser light scattering from a metal grating: it matches the experimental data by taking into account the finite refractive index of the metal supplied by measurements.[8–10] Liu and Hong proposed a general method for analyzing electromagnetic wave scattering from arbitrarily shaped two-dimensional periodic surfaces.[11] In 2003, Nakayama and Kashihara modified a spectral formalism to deal with transverse magnetic and transverse electric (TE) waves scattering from a finite periodic surface.[12–15] Comparing a finite periodic surface with an infinite periodic case, they proved that the relative powers of the diffraction beam are very similar to those in the case of the infinite periodic surface. By using the Fresnel phase approximation and receiver directivity approximations, Welton[16] analyzed the scattering by pressure-release sinusoidal surfaces in three dimensions. Furthermore, Ge numerically investigated the optical trapping properties of nanoparticles placed on a gold film with periodic circular holes.[17] In 2014, based on the Rayleigh hypothesis and Floquet's theorem, Huang and Dong[18,19] proposed a vector method for the problem of TE electromagnetic wave scattering by a one-dimensional periodic conducting surface.

Generally speaking, the existing literature mainly studied the periodic surface scattering in one aspect, but did not systematically and comprehensively explore the influence of various factors on the scattering of the periodic dielectric surface. These factors include the frequency of the incident wave, the

*Project supported by the National Natural Science Foundation of China (Grant Nos. 61571355, 61801349, and 61601355).
†Corresponding author. E-mail: wuzhs@mail.xidian.edu.cn
© 2019 Chinese Physical Society and IOP Publishing Ltd

incident angle, polarization modes, the amplitude and period of the periodic surface, permittivity, and so on.

In microwave remote sensing, especially in the detection of a ship wake by space-borne radar, the effective calculation of the scattering cross section of a periodic structure in a large area is particularly important.[20–25] In the previous literature, the scattering cross section was mostly used to simulate the scattering of the periodic surface with a finite length and small area. However, so far, for an infinite or extremely large area, the formula for the scattering cross section has not been referred to.

In this context, the scattering from dielectric periodic surfaces with several important factors is studied. Moreover, the scattering cross section of the infinite periodic surface is derived by improving the scattering cross section of the finite length case so that the scattering problems of the infinite and the long, finite period surfaces can be unified under a reasonable approximation.

The structure of the paper is as follows. In Section 2, the Fourier expression of the scattering field of the periodic surface is obtained by Huygens's principle and Floquet's theorem. Using the extended boundary condition method (EBCM) and the T-matrix method, the scattering amplitude coefficient is solved. The scattering cross section formula for the infinite periodic dielectric surface is derived in Section 3, which is approximated reasonably from the finite periodic surface under certain conditions. In Section 4, the correctness of the above algorithm is verified by the energy conservation law and experimental data. Focusing on the representative sinusoidal surface, numerical results of the scattering rate, transmittance, as well as scattering intensity are presented and discussed. Furthermore, the effect of the total length of the periodic surface on scattering is analyzed. Lastly, several conclusions are given in Section 5.

2. Scattering of the periodic surface

2.1. Formula of the scattering field

Let us consider the scattering of a plane wave by a finite periodic surface,[4,6] as shown in Fig. 1. The surface corrugation is written as

$$z = f(x) = u(x|W) f_P(x), \tag{1}$$

where $f_P(x)$ is the periodic function with a period P, and W is the total length of the periodic surface. Here,

$$f_P(x) = f_P(x+P), \tag{2}$$

and $u(x|W)$ is a gate function with the width W

$$u(x|W) = \begin{cases} 0, & |x| > W/2, \\ 1, & |x| < W/2. \end{cases} \tag{3}$$

For convenience, k_P and k_W are set as

$$k_P = \frac{2\pi}{P}, \quad k_W = \frac{2\pi}{W}. \tag{4}$$

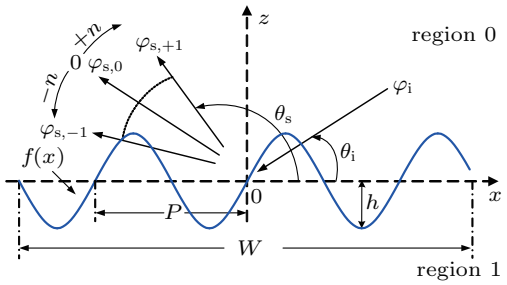


Fig. 1. Scattering of a plane wave by a periodic dielectric surface.

We denote the y component of the electric field by $\psi(x,z)$, which satisfies the Helmholtz equation in the region $z > f(x)$ and the Dirichlet condition on the surface $z = f(x)$:

$$\left[\frac{\partial^2}{\partial x^2} + \frac{\partial^2}{\partial z^2} + k^2\right] \psi(x,z) = 0, \tag{5}$$

$$\psi(x,z)|_{z=f(x)} = 0. \tag{6}$$

Here, $k = 2\pi/\lambda$ is the wavenumber, and λ is the wavelength. The incident plane wave $\psi_i(x,z)$ is written as

$$\psi_i(x,z) = \mathrm{e}^{-\mathrm{i}k_{ix}x}\mathrm{e}^{-\mathrm{i}\beta_0(k_{ix})z}, \quad k_{ix} = k\cdot\cos\theta_i, \tag{7}$$

$$\beta_m(k_{ix}) = \beta_0(k_{ix}+mk_P) = \sqrt{k^2-(k_{ix}+mk_P)^2},$$
$$\mathrm{Im}[\beta_m(k_{ix})] \geqslant 0, \quad m = 0, \pm1, \pm2, L, \tag{8}$$

where θ_i is the incident angle, Im stands for the imaginary part, and the electric field amplitude of the incident wave is $E = 1$. Since the surface is flat for $|x| > W/2$, the y component of the electric field is shown as

$$\psi(x,z) = \mathrm{e}^{-\mathrm{i}k_{ix}x}\left[\mathrm{e}^{-\mathrm{i}\beta_0(k_{ix})z} - e^{i\beta_0(k_{ix})z}\right] + \psi_s(x,z), \tag{9}$$

which is the sum of the incident plane wave, specular reflection, and scattered wave $\psi_s(x,z)$ due to surface deformation. By use of the periodic Fourier transform,[26] the scattering field has an extended Floquet form

$$\psi_s(x,z) = \int_{-\infty}^{\infty} A(s)\mathrm{e}^{-\mathrm{i}(k_{ix}+s)x+\mathrm{i}\beta_0(k_{ix}+s)z}\mathrm{d}s \tag{10}$$

$$= \sum_{m=-\infty}^{\infty} \psi_m(x,z), \tag{11}$$

where equations (10) and (11) hold for $|z| > \max[f(x)]$. $A(s)$ is the spectral amplitude. Equation (11) is the extended Floquet form, where $\psi_m(x,z)$ is the m-th order diffraction beam given by[26]

$$\psi_m(x,z) = \frac{1}{k_P}\int_{-\pi/P}^{\pi/P} A_m(s) \times \mathrm{e}^{-\mathrm{i}(k_{ix}+s+mk_L)x} \times \mathrm{e}^{\mathrm{i}\beta_m(k_{ix}+s)z}\mathrm{d}s. \tag{12}$$

Here, it is worthwhile to note that $A_m(s)$ is related to the spectral amplitude $A(s)$ as follows:

$$A_m(s) = k_P \cdot A(s+mk_P)u(s|k_P). \tag{13}$$

By substituting Eq. (13) into Eq. (11), we obtain

$$\psi_s(x,z) = \sum_{m=-\infty}^{\infty} \psi_m(x,z) = \frac{e^{-ik_{ix}x}}{k_P} \sum_{-\infty}^{\infty} e^{-imk_P x} \times \int_{-\pi/P}^{\pi/P} A_m(s) e^{-isx+i\beta_m(k_{ix}+s)z} ds. \tag{14}$$

It is worth noting that equation (14) satisfies Eq. (5) and the radiation condition at $z \to \infty$ term by term. $A_m(s)$ is a complex amplitude of a plane wave propagating in the direction $\boldsymbol{k}$:

$$\boldsymbol{k} = -(s+k_{ix}+mk_P)\boldsymbol{e}_x + \beta_m(s+k_{ix})\boldsymbol{e}_z. \tag{15}$$

In other words, $A_m(s)$ is the amplitude of a plane wave scattered into the θ_s direction, where θ_s is given by

$$\cos\theta_s = -\left(\cos\theta_i + \frac{s}{k} + m\frac{\lambda}{P}\right). \tag{16}$$

If $s = 0$, equation (16) degenerates the famous grating formula

$$\cos\theta_m = -\left(\cos\theta_i + m\frac{\lambda}{P}\right), \tag{17}$$

where m stands for the diffraction order. Since m is an integer, and because the incident angle, wavelength, and surface period length are constant, it can be deduced that the scattering intensity will take an extreme value at θ_m. Equation (14) is a product of the exponential phase factor $\exp(-ik_{ix}x)$ and a harmonic series that is a "Fourier series" given by band-limited Fourier integrals. When W goes to infinity and equation (1) becomes infinitely periodic, the amplitude function turns into

$$A_m(s) = k_P \cdot \hat{A}_m \delta(s), \quad W \to \infty, \tag{18}$$

where $\hat{A}_m$ is a diffraction amplitude, and $\delta(s)$ is Dirac's delta function. Hence, equation (14) degenerates into the famous Floquet form for the periodic grating. Therefore, equation (14) is regarded as an extension of the Floquet form and is called the extended Floquet form[6,9]

$$\psi_s = e^{-ik_{ix}x} \sum_{-\infty}^{\infty} \hat{A}_m e^{-imk_P x} e^{i\beta_m(k_{ix})z}, \quad W \to \infty. \tag{19}$$

When W is much larger than the wavelength, however, $A_m(s)$ is expected to be a localized function taking a large value only at $s \approx 0$. This implies that $\psi_m(x,z)$ is a beam whose main lobe scatters along the direction θ_m determined by Eq. (17). Thus, $\psi_m(x,z)$ is called the m-th order diffraction beam.

2.2. Scattering cross section

Physically, the diffracted waves are radiated from the corrugated part of the surface, and hence they exist only at limited regions in space. Considering the far field case, the scattering cross section can be obtained by solving the integrals in Eq. (14) with the saddle point method.

We denote a scattering angle by θ_s (see Fig. 1) in the polar coordinate:

$$x = r\cos\theta_s, \quad z = r\sin\theta_s. \tag{20}$$

Then, using the saddle point method, the approximated form of Eq. (14) is

$$\psi_s(r\cos\theta_s, r\sin\theta_s) \approx \frac{k\sin\theta_s}{k_L}\sqrt{\frac{2\pi}{kr}} e^{ikr-i\pi/4} \sum_{m=-\infty}^{\infty} A_m(-k\cos\theta_s - k_{ix} - mk_P) \times u(-k\cos\theta_s - k_{ix} - mk_P|k_P). \tag{21}$$

From this relation, the scattering cross section $\sigma(\theta_s|\theta_i)$ is obtained and expressed as

$$\sigma(\theta_s|\theta_i) = \lim_{r\to\infty} 2\pi\frac{kr}{kW}|\psi_s(r\cos\theta_s, r\sin\theta_s)|^2 \approx \frac{(2\pi)^2 k}{k_P^2 W} \sum_{m=-\infty}^{\infty} \sin^2\theta_s u(-k\cos\theta_s - k_{ix} - mk_P|k_P) \times |A_m(-k\cos\theta_s - k_{ix} - mk_P)|^2, \tag{22}$$

which is a non-dimensional quantity divided by the corrugation width W. Let $W = n_W P$, and n_W is a positive integer. When $n_W \to \infty$, W tends to infinity. From Eqs. (18) and (22), the bistatic scattering coefficient of the periodic surface in a large area can be obtained:

$$\sigma(\theta_s|\theta_i) = \frac{(2\pi)^2 k}{W}\sin^2\theta_s \times \sum_{m=-\infty}^{\infty} u(-k\cos\theta_s - k_{ix} - mk_P|k_P) \times \left|\hat{A}_m \delta(-k\cos\theta_s - k_{ix} - mk_P)\right|^2. \tag{23}$$

For the convenience of calculation, the Dirac function $\delta(s)$ is approximated as follows:[6]

$$\delta(kWs) \to \frac{kW}{2\pi}\frac{\sin(kWs/2)}{kWs/2}, \quad W \to \infty. \tag{24}$$

As we can see in Eq. (23), the scattering field amplitude $\hat{A}_m$ is an important factor in the formula of the scattering cross section of the infinite periodic surface.

2.3. Calculation of scattering field amplitude coefficient $\hat{A}_m$

When $W \to \infty$, by substituting Eq. (18) in Eq. (12) and utilizing the selectivity of the Dirac function, we can obtain

$$\psi_m(x,z) = \int_{-\pi/P}^{\pi/P} \hat{A}_m \delta(s) e^{-i(k_{ix}+s+mk_L)x} e^{i\beta_m(k_{ix}+s)z} ds = \hat{A}_m e^{-i(k_{ix}+mk_L)x+i\beta_m(k_{ix})z}. \tag{25}$$

Using Floquet's theorem and Huygens's principle, the scattering propagation models are derived. The scattering amplitude $\hat{A}_m$, or diffraction amplitude, is acquired by the EBCM and the T-matrix method[9,10]

$$\begin{aligned}\boldsymbol{A} &= [\hat{A}_m] = -\boldsymbol{Q}_D^+ \cdot \boldsymbol{\beta}^s - \boldsymbol{Q}_N^+ \cdot \boldsymbol{\alpha}^s,\\ \boldsymbol{B} &= [\hat{B}_n] = -\boldsymbol{Q}_{D1}^- \cdot \boldsymbol{\beta}^s - \boldsymbol{Q}_{N1}^- \cdot \boldsymbol{\alpha}^s,\end{aligned} \tag{26}$$

where matrix $\boldsymbol{A}$ is upward-going field amplitudes and $\boldsymbol{B}$ is downward-going field amplitudes. $\boldsymbol{\alpha}^s$ and $\boldsymbol{\beta}^s$ can be obtained by the following matrix equations:

$$-\begin{bmatrix} \boldsymbol{Q}_N^- & \boldsymbol{Q}_D^- \\ \boldsymbol{Q}_{N1}^+ & \boldsymbol{Q}_{D1}^+ \end{bmatrix} \begin{bmatrix} \boldsymbol{\alpha}^s \\ \boldsymbol{\beta}^s \end{bmatrix} = \begin{bmatrix} \boldsymbol{a} \\ \boldsymbol{0} \end{bmatrix}, \tag{27}$$

$$a_n = \delta_{n0}\sqrt{k_z}E_0, \tag{28}$$

where $\boldsymbol{Q}_D^{\pm}$ and $\boldsymbol{Q}_N^{\pm}$ are Dirac matrices and Neumann matrices, respectively, under different boundary conditions:

$$\begin{aligned}\left[Q_D^{\pm}\right]_{mn} &= \pm\frac{1}{P}\int_P \mathrm{d}x \frac{\mathrm{e}^{\mathrm{i}k_n^{\pm}\cdot r}}{\sqrt{k_{\mathrm{zm}}}}\mathrm{e}^{\mathrm{i}(k_{\mathrm{ix}}+nk_P)x},\\ \left[Q_N^{\pm}\right]_{mn} &= \pm\frac{-\mathrm{i}}{P}\int_P \mathrm{d}S\hat{n}\cdot\left(\nabla_{\mathrm{s}}\frac{\mathrm{e}^{\mathrm{i}k_m^{\pm}\cdot r}}{\sqrt{k_{\mathrm{zm}}}}\right)\mathrm{e}^{\mathrm{i}(k_{\mathrm{ix}}+nk_P)x},\\ \left[Q_{D1}^{\pm}\right]_{mn} &= \pm\frac{1}{P}\int_P \mathrm{d}x \frac{\mathrm{e}^{\mathrm{i}k_{1n}^{\pm}\cdot r}}{\sqrt{k_{1zm}}}\mathrm{e}^{\mathrm{i}(k_{\mathrm{ix}}+nk_P)x},\\ \left[Q_{N1}^{\pm}\right]_{mn} &= \pm\frac{-\mathrm{i}}{P}\int_P \mathrm{d}S\hat{n}\cdot\left(\nabla_{s}\frac{\mathrm{e}^{\mathrm{i}k_{1m}^{\pm}\cdot r}}{\sqrt{k_{1zm}}}\right)\mathrm{e}^{\mathrm{i}(k_{\mathrm{ix}}+nk_P)x},\end{aligned} \tag{29}$$

$$\begin{aligned}k_{zm} &= \beta_m(k_{\mathrm{ix}}) = \sqrt{k^2-(k_{\mathrm{ix}}+mk_P)^2},\\ k_{1zm} &= \sqrt{k_1^2-(k_{\mathrm{ix}}+mk_P)^2},\\ k_1 &= k/\sqrt{\mu_{\mathrm{r}}\varepsilon_{\mathrm{r}}}k_n^{\pm} = \hat{x}k_{xn}\pm\hat{z}k_{zn}.\end{aligned} \tag{30}$$

When the periodic surface is a sine function,

$$f_P(x) = h\sin(\frac{2\pi}{P}x), \tag{31}$$

where the amplitude is h, and the period is P. Then the Q-matrix can be written as

$$\begin{aligned}\left[Q_D^{\pm}\right]_{mn} &= \pm\frac{1}{\sqrt{k_{zm}}}(\pm\mathrm{i})^{|m-n|}J_{|m-n|}(k_{zm}h),\\ \left[Q_N^{\pm}\right]_{mn} &= \pm\frac{\left(-k^2+k_{xm}k_{xn}\right)}{k_{zm}P\sqrt{k_{zm}}}(\pm\mathrm{i})^{|m-n|}J_{|m-n|}(k_{zm}h),\\ \left[Q_{D1}^{\pm}\right]_{mn} &= \pm\frac{1}{\sqrt{k_{1zm}}}(\pm\mathrm{i})^{|m-n|}J_{|m-n|}(k_{1zm}h),\\ \left[Q_{N1}^{\pm}\right]_{mn} &= \frac{-k_1^2+k_{1xm}k_{1xn}}{k_{1zm}P\sqrt{k_{1zm}}}(\pm\mathrm{i})^{|m-n|}J_{|m-n|}(k_{1zm}h).\end{aligned} \tag{32}$$

According to the above method, we can determine $\hat{A}_m$ and obtain the bistatic scattering coefficient of the periodic surface $\sigma(\theta_{\mathrm{s}}|\theta_{\mathrm{i}})$ from Eq. (23).

3. Scattering and transmission power of the periodic dielectric surface

When the incident wave irradiates on the surface of the periodic medium, some parts of the energy are reflected or scattered, and other parts are transmitted or absorbed by the medium. Here, we call the specular reflection and the scattered wave as the scattering wave, and call the wave transmitted into the medium and absorbed by the medium as the transmission wave.

When the medium in region 1 (as shown in Fig. 1) is lossless, the scattering power P_m^{s} and the transmission power P_n^{t} of the TE wave in the m-th-mode (or nth-mode) are

$$P_m^{\mathrm{s}} = \frac{1}{2}\mathrm{Re}\frac{\omega k_{zm}}{k^2}\varepsilon\frac{|A_m|^2}{\sqrt{1-\cos^2\theta_m}} = \frac{\omega\varepsilon}{2k}|A_m|^2, \tag{33}$$

$$P_n^{\mathrm{t}} = \frac{1}{2}\mathrm{Re}\frac{\omega k_{1zn}}{k_1^2}\varepsilon_1\frac{|B_n|^2}{\sqrt{1-\cos^2\theta_n'}}\mathrm{e}^{2\mathrm{Im}[k_{1zn}]z} = \frac{\omega\varepsilon_1}{2k_1}|B_n|^2. \tag{34}$$

Supposing the amplitude of the incident wave is E_0, then the incident wave power is

$$P_{\mathrm{inc}} = \frac{1}{2}\frac{\omega\varepsilon}{k^2}E_0^2. \tag{35}$$

Hence, the efficiency of scattering and transmission is

$$s_\alpha = \sum_m P_m^{\mathrm{s}}/P_{\mathrm{inc}}t_\alpha = \sum_n P_n^{\mathrm{t}}/P_{\mathrm{inc}}. \tag{36}$$

For the lossless medium, the power relation is satisfies the energy conservation law

$$\sum_m P_m^{\mathrm{s}}/P_{\mathrm{inc}} + \sum_n P_n^{\mathrm{t}}/P_{\mathrm{inc}} = 1, \tag{37}$$

where the summation is over all propagating modes. As a necessary condition, equation (37) is often used to prove the accuracy of the numerical results.

Roughly speaking, the total power of scattering and the power P_m^{s} are proportional to W because the scattering takes place at the corrugated part of the surface. Thus, the relative power P_m/P_{inc} is expected to become almost independent of W. This implies an expectation that the relative powers of diffraction beams are very similar to the diffraction powers for an infinite periodic surface.[13]

4. Results and discussions

In this section, the scattering and transmission power and scattering intensity distribution of the sinusoidal, infinite dielectric surface are simulated. By changing the frequency of the incident wave, incident angle, periodic surface amplitude, period length, and dielectric coefficient, numerical simulation is carried out to explore the influence of various factors on the scattering of the periodic surface.

4.1. Verification of the above method

The following work is a validation of the method described in Section 2.

4.1.1. Verification of the method by the energy conservation law

Figure 2 shows the variation of the scattering power and transmission power with the incident angle under different conditions, and the detailed parameters are shown in Table 1. From the general trend of change, the scattering efficiency decreases with the increase in incident angle. Conversely, transmittance increases with the increase in incident angle in the range of $0° < \theta_i < 90°$. However, the scattering efficiency varies locally at partial incident angles. For example, in Fig. 2(d), the efficiencies of scattering and transmission reaches their extremes when $\theta_i = 25°$, 37°, and 45°. As the "total" curve shows, the sum of scattering and transmission is 1, which satisfies the energy conservation law.

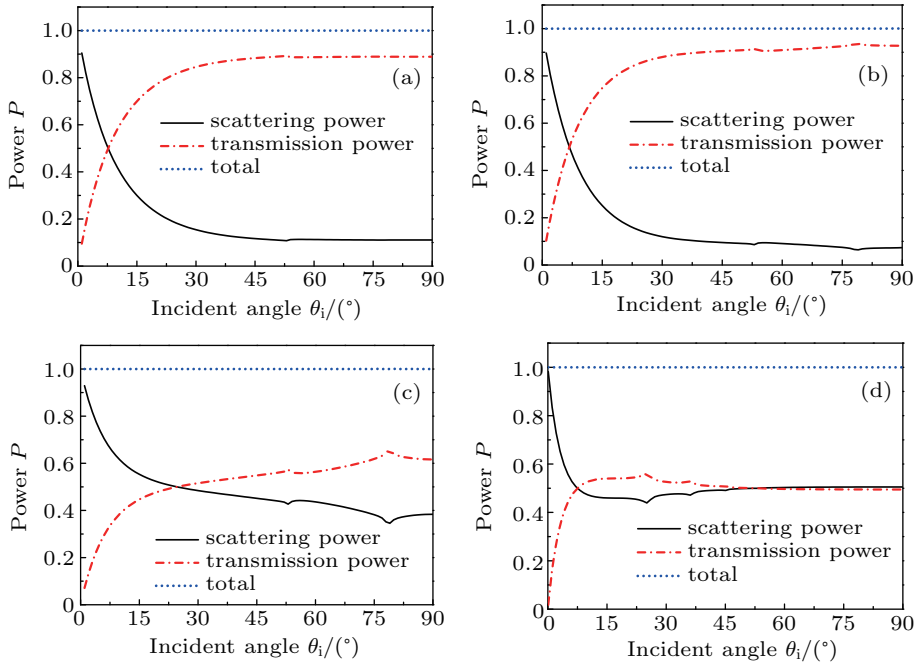


Fig. 2. Variation of scattering power and transmission power with incident angle.

Table 1. The parameter list.

	Fig. 2(a)	Fig. 2(b)	Fig. 2(c)	Fig. 2(d)
E	1	1	1	1
h/λ	0.1	0.4	0.4	0.4
P/λ	2.5	2.5	2.5	10
ε_{r1}	1	1	1	1
ε_{r2}	4	4	35	35

It is worth noting that the periodic surface will degenerate to a plane when $h = 0$. The simulation data can be compared with the consequence of the Fresnel reflection formula to further verify the correctness of the algorithm.

The coefficients of Fresnel reflection and transmission are expressed as

$$R = \frac{1 - p_{0t}}{1 + p_{0t}}, \quad T = \frac{2}{1 + p_{0t}}, \tag{38}$$

where $p_t = \mu k_{tz}/(\mu k_z)$, k_z and k_{tz} are the components of the incident and transmitted wave numbers along the normal direction of the plane, respectively (see Ref. [27] for details). The corresponding power reflectivity and power transmissivity are given as

$$r = |R|^2, \quad t = p_{0t}|T|^2. \tag{39}$$

Equation (39) can be used to compare with the above method. As shown in Fig. 3, where $\varepsilon_r = 4$, the results of the two methods are in good agreement, and the variation of scattering (reflection) and transmission power still conform to the law of energy conservation. Thus, the above algorithm is effective.

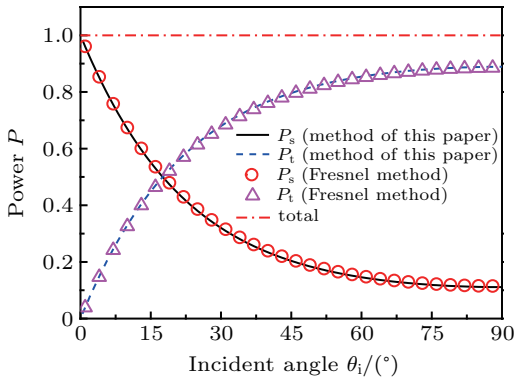


Fig. 3. Comparison of the method of this paper with the Fresnel method.

4.1.2. Verification of the method by comparing with experimental data

The effect of the row structure on the microwave emission from a bare agricultural field has been reported together with

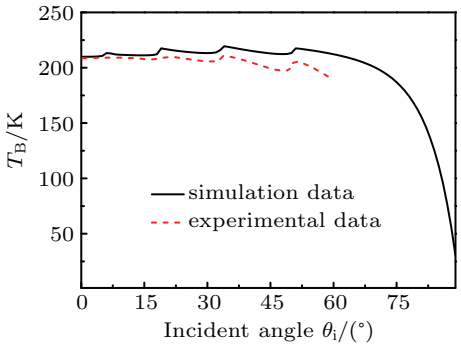


Fig. 4. Brightness temperature as a function of incident angle θ_i.

the soil moisture contents for the measured data.[7,28] The theoretical results are illustrated for a sinusoidal surface in Fig. 4 at a frequency of 1.4 GHz. The periodic surface has a height $h = 0.1$ m and a period $P = 0.95$ m, and can be approximated by a sinusoidal function. For the upper medium, let $\varepsilon = \varepsilon_0$ and $\mu = \mu_0$. T_B is the brightness temperature, and $T_B = T(1 - P_r)$ by definition. P_r denotes the reflection power or scattering power.

In Fig. 4, the radiometer observation angles are perpendicular to the row direction. The soil moisture content is 29% by dry weight at the top 0 to 5 cm and becomes drier with depth. The complex permittivity is approximately $(10 + i2)$. We see that the simulation data of brightness temperatures T_B for the horizontal polarization are similar to the experimental data from 0° to 60°.

Besides, we observe that the T_B curves for the periodic surface are not smoothly varying. There are kinks appearing at observation angles θ near 6°, 19°, 34°, and 51°. The corresponding change in T_B may be as high as 10 K. Such a phenomenon is caused by the redistribution of the scattered power during the course of the disappearance and appearance of the propagating Floquet modes.

4.2. The effect of W on periodic surface scattering

Theoretically, when using Floquet's theory to calculate the scattering of an infinite periodic surface, the scattering wave propagates in discrete Floquet modes. This means that the distribution of the scattering intensity has values just at the angles corresponding to the Floquet mode (as shown in Table 2). However, the distribution of scattering intensity of the finite periodic surface is continuous.

As shown in Fig. 5, under the same incident condition, as n_W increases, the periodic surface length W increases, and the distribution of the scattering intensity is only concentrated at the angle corresponding to the Floquet modes. For example, when $n_W = 5000$, although the scattering cross section is continuous with the change in the scattering angle, the scattering intensity is obviously concentrated at the corresponding Floquet mode angles, and the scattering intensity values at other scattering angles are so small that they can be negligible.

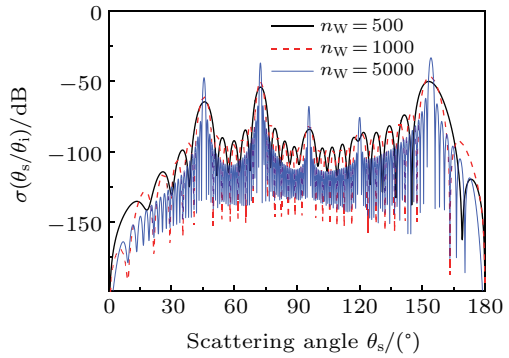


Fig. 5. Scattering cross section under different lengths of periodic surface ($W = n_W P$).

Therefore, by using the above method in practical calculation, regardless of a finite or an infinite periodic surface, reasonable results can be obtained through taking the appropriate value of W. This is also one of the points of this work.

4.3. Influencing factors of scattering power

Figure 6 presents the comparison of the relative scattering power of the periodic surfaces under different conditions, with incident angle.

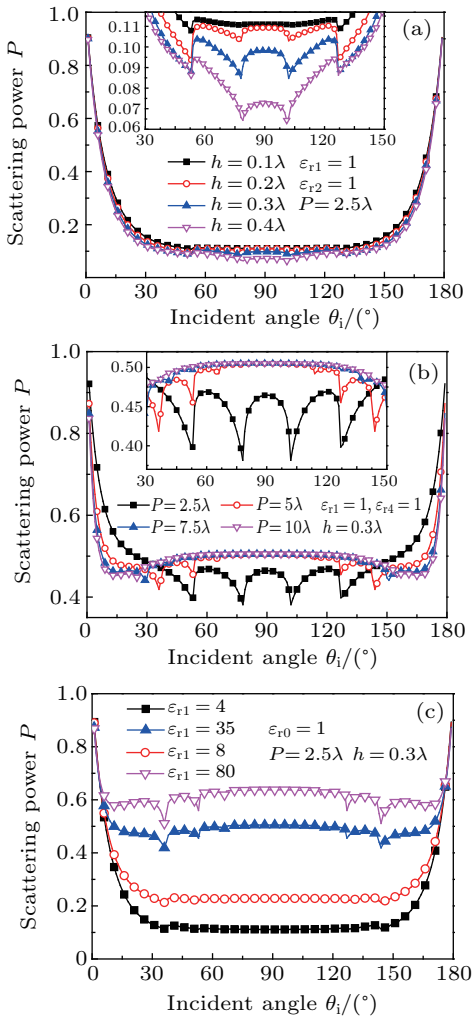


Fig. 6. The variation of scattering power with incident angle under different conditions. (a) Scattering power under different amplitudes h. (b) Scattering power under different periods P. (c) Scattering power under different permittivity ε_{r1}.

Figure 6(a) compares the relative scattering power of different periodic surface amplitudes with the incident angle. It can be seen that the relative scattering power at different amplitudes h has little difference when $0^\circ < \theta_i < 30^\circ$ and $150^\circ < \theta_i < 180^\circ$. However, the difference is obvious at the region of $30^\circ < \theta_i < 150^\circ$, that is, the larger the amplitude h, the smaller the scattering power at the same incident angle θ_i.

Figure 6(b) compares the relative scattering power with the incident angle under different periods P. It can be seen that the scattering power decreases at $0^\circ < \theta_i < 35^\circ$ and $145^\circ < \theta_i < 180^\circ$ with an increase in period P. However, when $35^\circ < \theta_i < 145^\circ$, the trend is the opposite.

According to Figs. 6(a) and 6(b), the larger the amplitude h and the smaller the period P, which means that the periodic surface is rougher, the effect of scattering is more obvious, and the oscillation of the relative scattering power curve is more evident.

Figure 6(c) compares the relative scattering power of different relative permittivity ε_{r1} with the incident angle. ε_{r1} is the relative permittivity of region 1. It can be seen that ε_{r1} has a positive correlation with the scattering power. When other conditions remain unchanged, the larger the permittivity, the greater the scattering power.

4.4. Analysis of scattering cross section

Using the formulae in Section 3, the scattering field of the dielectric periodic surface is calculated by Eq. (23). As shown in Fig. 7, the normalized bistatic scattering cross section $\sigma(\theta_s|\theta_i)$ under different surface amplitudes is calculated, where $\theta_i = 60^\circ$, and $P = 2.5\lambda$, and h takes 0, 0.05λ, 0.1λ, 0.2λ, 0.3λ, and 0.4λ, respectively.

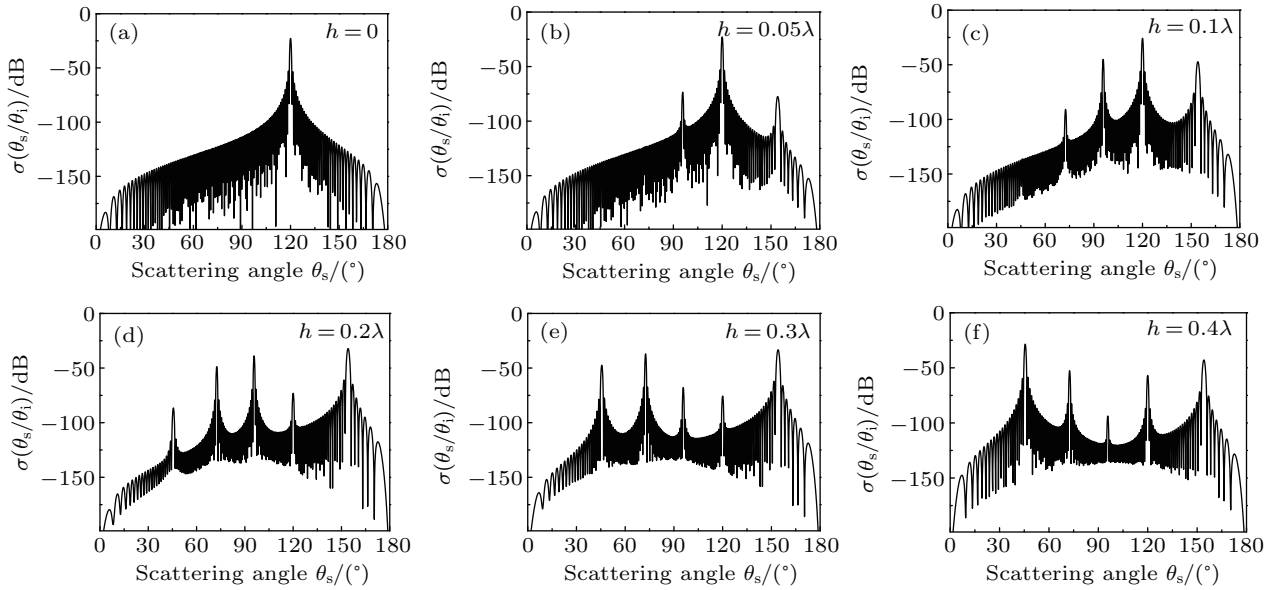


Fig. 7. Scattering cross section under different amplitudes h.

When $h = 0$, that is, when the interface is a plane, as shown in Fig. 1(a), the scattering intensity is concentrated only in the direction of $\theta_s = 120^\circ$, which means that there is no scattering, only specular reflection. This is in line with the actual situation.

Figures 7(b), 7(c), and 7(d) correspond to the cases of $h = 0.05\lambda$, 0.1λ, and 0.2λ, respectively. It can be seen that the maximum peak value of the scattering cross section is still at $\theta_s = 120^\circ$, which is the specular direction. However, the number of peaks increases sequentially: 3, 4, and 5, respectively. This shows that as the amplitude h of the periodic surface increases, the number of peaks of the scattering cross section increases, and the scattering is more obvious.

Besides, by comparing Figs. 7(d), 7(e), and 7(f), we can see that the maximum scattering cross section is no longer located in the specular direction ($\theta_s = 120^\circ$) when h continues to increase ($h = 0.2\lambda$, 0.3λ, and 0.4λ), even though the numbers of peaks are the same.

Generally, a larger amplitude h causes the surface to be rougher, thus enhancing the scattering effect. Furthermore, the corresponding scattering peaks and their positions (angles) are shown in Table 2, which agree with diffraction angles calculated by the grating formula (Eq. (17)).

Table 2. The m-th modes and the corresponding angles θ_{sm}.

m	θ_{sm}
−3	45.57°
−2	72.54°
−1	95.74°
0	120°
1	154.16°

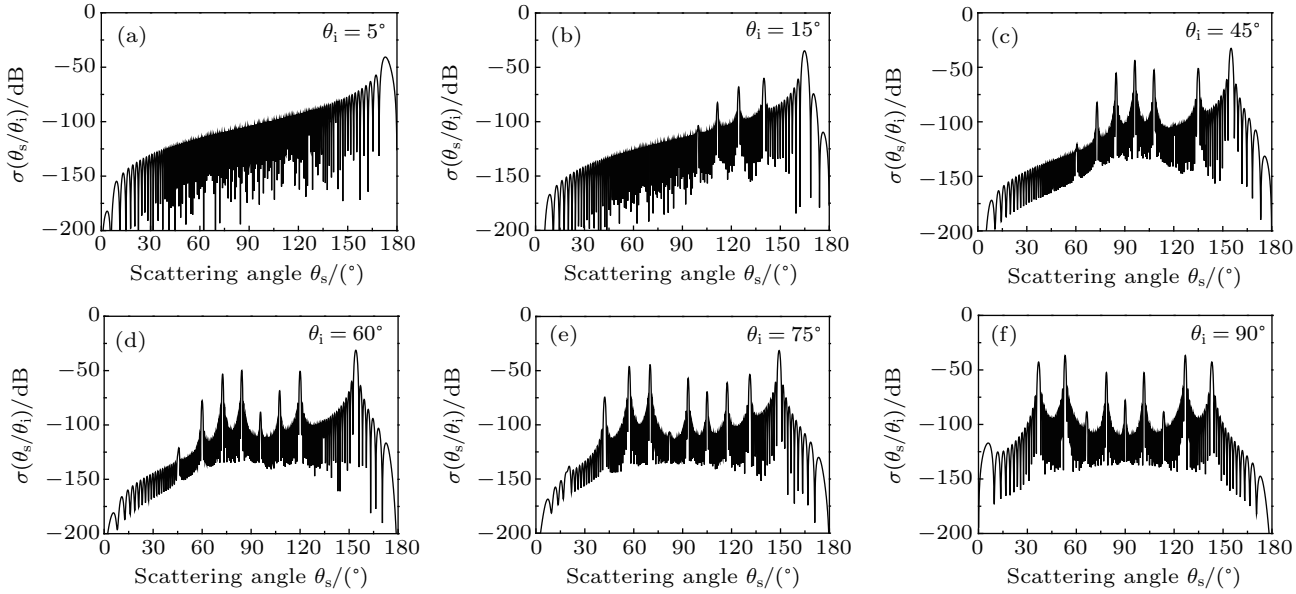


Fig. 8. Scattering cross section under different incident angles θ_i.

Figure 8 compares the normalized bistatic scattering cross section $\sigma(\theta_s|\theta_i)$ of periodic dielectric surfaces at different incident angles, where $P = 5\lambda$, $h = 0.4\lambda$, $\varepsilon_{r1} = 4$, and $E_0 = 1$.

It is evident from Figs. 8(a) and 8(b) that the scattering intensity is mainly concentrated on the specular direction when the incident angle θ_i is small (or in the case of small grazing angle). For example, when $\theta_i = 15°$, the maximum value of the peak value of the scattering cross section is at the angle of $\theta_s = 165°$.

With the increase in incident angle θ_i, the distribution of scattering intensity changes significantly. As shown in Figs. 8(c)–8(e), the number of peaks of the scattering cross section increases obviously, and the position of the maximum peak is no longer the specular position of the incident angle. For example, when $\theta_i = 45°$, the position of the maximum peak is at $\theta_s = 155.1°$, not 135°, which is in the specular direction of the incident angle. When $\theta_i = 60°$, the position of the maximum peak is at $\theta_s = 154.1°$, not 120°, which is in the specular direction of the incident angle.

Table 3. Angular locations of scattering cross section peaks.

	5°	15°	45°	60°	75°	90°
−9	36.5°	33.5°				
−8	52.9°	50.6°	26.8°			
−7	66.2°	64.3°	46.1°	25.8°		
−6	78.2°	76.5°	60.5°	45.6°	19.7°	
−5	89.9°	88°	73°	60°	42.2°	0.01°
−4	101.3°	99.6°	84.7°	72.5°	57.2°	36.9°
−3	113.3°	111.5°	96.1°	84.3°	70.1°	53.1°
−2	126.6°	124.5°	107.9°	95.7°	81.9°	66.4
−1	142.8°	134°	120.5°	107.5°	93.4°	78.5°
0	175°	165°	135°	120°	105°	90°
1			155.1°	134.4°	117.3°	101.5°
2				154.2°	131.2°	113.6°
3					149.2°	126.9°
4						143.1°

When θ_i continues to increase until it is close to the vertical incidence, the intensity distribution of the scattering cross section is stable, which means that the scattering effect on the periodic dielectric surface is significant.

Table 3 records the scattering wave modes m and positions of peaks at different incident angles shown in Fig. 5.

5. Conclusions

In this paper, the problem of scattering from the periodic surface is discussed in detail. With the large length of the periodic surface, the formula for the electromagnetic scattering cross section of the finite periodic surface can be approximated and expanded, which makes it possible to calculate the scattering cross section of infinite periodic surfaces. Moreover, the scattering calculation methods of infinite and long, finite surfaces are unified by a reasonable approximation. In addition, the correctness of the algorithm is verified by means of the energy conservation law and experiments performed using the brightness temperature. The effects of various factors on scattering characteristics are comprehensively analyzed. These factors include the geometry of the periodic surface (amplitude and period), dielectric parameters, wavelength, and incident angle.

The simulation results indicate that the scattering rate of the periodic surface increases with an increase in dielectric parameters; the opposite is seen for transmission. The relative geometric parameters (P/λ and h/λ) of the surface together with the incident angle significantly affect the scattering intensity distribution. In general, with the increase in surface roughness and incident angle, the number of scattering intensity peaks increases, which means that the scattering effects are more notable.

Through the above work, we find that the dielectric periodic surface has a significant effect on the scattering rate and transmittance. The period and amplitude of the surface determine the number of scattering intensity peaks, and also influence the scattering intensity distribution with incident angle. The work in this paper can be used for the recognition of special targets, such as a ship wake or agricultural field, and it will be studied further in the future.

References

[1] Nordam T, Letnes P A, Simonsen I and Maradudin A A 2014 *J. Opt. Soc. Am. A* **31** 1126
[2] Tishchenko A V 2010 *Opt. Photon. News* **21** 50
[3] Uretsky J L 1965 *Ann. Phys.* **33** 400
[4] Desanto J A 1974 *J. Acoust. Soc. Am.* **56** 1195
[5] Desanto J A 1981 *Radio Sci.* **16** 1315
[6] Jordan A K and Lang R H 1979 *Radio Sci.* **14** 1077
[7] Wang J R, Newton R W and Rouse J W 1980 *IEEE Trans. Geosci. Remote Sens.* **GE-18** 296
[8] Chuang S L and Kong J A 1981 *Proc. IEEE* **69** 1132
[9] Chuang S L and Kong J A 1982 *Radio Sci.* **17** 545
[10] Kong J A, Lin S L and Chuang S L 1984 *IEEE Trans. Geosci. Remote Sens.* **GE-22** 377
[11] Liu K and Hong W 1992 *Int. J. Infrared Millimeter Waves* **13** 1647
[12] Kashihara A and Nakayama J 2006 *Electron. Commun. Jpn. Part 2* **89** 10
[13] Nakayama J and Yoshinobu K 2003 *IEICE Trans. Electr.* **86** 1098
[14] Nakayama J and Tsuji H 2002 *IEICE Trans. Electr.* **85** 1808
[15] Nakayama J 2000 *IEICE Trans. Electr.* **88** 481
[16] Welton P J 2012 *J. Acoust. Soc. Am.* **131** 54
[17] Ge C X, Wu Z S, Bai J and Gong L 2019 *Chin. Phys. B* **28** 024203
[18] Huang Q, Dong T L, Chen B, Li Q and Chen P 2014 *J. Quant. Spectrosc. Radiat. Transfer* **134** 85
[19] Huang Q, Dong T, Chen B, Li Q, Tian J and Chen P 2014 *J. Opt. Soc. Am. A* **31** 2321
[20] Reed A M, Beck R F, Griffin O M and Peltzer R D 2002 *Annu. Rev. Fluid Mech.* **34** 469
[21] Tunaley J K, Buller E H, Wu K and Rey M T 1991 *IEEE Trans. Geosci. Electron.* **29** 149
[22] Oumansour K, Wang Y and Saillard J 1996 *IEE Proc. Radar Sonar and Nav.* **143** 275
[23] Zilman G, Zapolski A and Marom M 2004 *IEEE Trans. Geosci. Electron.* **42** 2335
[24] Tings B and Velotto D 2018 *Int. J. Remote Sens.* **39** 4451
[25] Veysoglu M E, Yueh H A, Shin R T and Kong J A 1991 *J. Electromagn. Waves Appl.* **5** 267
[26] Longman I M 1986 *Appl. Numer. Math.* **2** 135
[27] Kong J A 1975 *Theory of Electromagnetic Waves* (New York: Wiley) p. 13
[28] Tsang L, Kong J A, Ding K H and Ao C O 2004 *Scattering of Electromagnetic Waves: Numerical Simulations* (New York: Wiley) p. 83